Using Circuit Theory and Swarm Intelligence for the Design and Optimization of Energy Harvesters for Ambient Mechanical Vibrations

Using Circuit Theory and Swarm Intelligence for the Design and Optimization of Energy Harvesters for Ambient Mechanical Vibrations

Kailing Song
Dept. of Electronics and Telecommunications
Politecnico di Torino, Turin, Italy
kailing.song@polito.it

Michele Bonnin
Dept. of Electronics and Telecommunications
Politecnico di Torino, Turin, Italy
michele.bonnin@polito.it

Fabio L. Traversa
MemComputing Inc.
San Diego, CA, USA
ftraversa@memcpu.com

Fabrizio Bonani
Dept. of Electronics and Telecommunications
Politecnico di Torino, Turin, Italy
fabrizio.bonani@polito.it

***Abstract*—We consider the model of a networked energy harvester for ambient dispersed vibrations, based on coupled mechanical resonators and a piezoelectric transduction mechanism. The networked harvester is equivalent to a mechanical filter that can be optimized for broadband energy harvesting. Using mechanical-to-electrical analogies, we derive an equivalent circuit model for the energy harvester, and we calculate the transfer function, output voltage, average harvested power and power efficiency in the frequency domain. We discuss the problem of the energy harvester optimization. Because analytical formulas for the objective function and its derivatives are not available, we apply a gradient-free method, based on Particle Swarm Optimization, to find the network parameters that maximize the scavenged energy. We show that, after proper optimization, the networked energy harvester collects significant more power than a single degree-of-freedom energy harvester.**

I. Introduction

Energy harvesting (EH) refers to the process of capturing ambient dispersed energy, which would otherwise be lost, and recycling it into usable electrical power. EH is expected to have a major impact in areas such as sensor and actuator networks, wearable electronics, and smart city systems, where replacing batteries is expensive or impractical due to remote or hard-to-reach locations. EH also holds significant potential for the Internet of Things (IoT), which relies on compact, durable, and energy-efficient devices. In these contexts, conventional batteries may be unsuitable, as their size and weight can limit the miniaturization and operational lifetime required for these technologies. By reducing or even eliminating reliance on batteries and external energy supplies, EH enables more sustainable and maintenance-free solutions, making it particularly valuable for compact, remote, or difficult-to-access applications [1]–[4].

Viable energy sources for EH include solar radiation, wind, thermal gradients, mechanical vibrations, and even radio-frequency emissions. While solar and wind-based harvesting are well-established and continue to advance, they are primarily suited for outdoor applications and often require large-scale infrastructure. In many practical cases, harvesting small amounts of energy is sufficient to power miniaturized devices such as wireless sensors, wearable technologies, or other low-power systems. Among the other sources, ambient mechanical vibrations are particularly promising for EH because they are abundant, relatively easy to harvest, and offer comparatively high energy density. Parasitic vibrations can originate from a wide range of sources, including household appliances, industrial equipment, vehicle motion, human activity, or environmental phenomena such as wind. Their frequency spectrum typically ranges from a few hertz, as in human motion, to several kilohertz, as in acoustic waves [5]–[7].

The typical energy harvester for mechanical vibrations consists of two main components: an oscillating structure that captures kinetic energy from vibrations, and a transducer that converts this energy into the electrical output. The oscillating structure is often modeled as a mass-spring system, sometimes complemented by a dampener to account for energy losses due to friction. This system behaves as a mechanical resonator with a defined natural frequency, at which the oscillation amplitude – and thus the harvested power – is maximized. However, performance decrease sharply at frequencies away from resonance, meaning that when ambient vibrations span a broad frequency range, only a small fraction of the available energy is actually harvested.

One strategy to enhance the performance of vibration energy harvesters is the use of nonlinear resonators. Unlike linear systems, nonlinear resonators often exhibit hysteresis, which broadens their operational bandwidth, albeit at the cost of a

reduced peak amplitude in the frequency response [8]–[11]. Another important characteristic of nonlinear devices is multi-stability, where multiple stable states can coexist. Transitions between these states can induce large oscillations, increasing power generation [12]–[14]. However, the inherent complexity of nonlinear dynamics complicates analysis, making the design and optimization of such harvesters more challenging [15]–[18].

In recent works, we proposed a solution to increase the harvested power based on the application of impedance matching [19], [20]. Impedance matching involves inserting a matching network between the transducer and the load to minimize the impedance mismatch between the mechanical and electrical domains. This can significantly improve both the extracted power and overall conversion efficiency. The approach is versatile, applicable to both linear and nonlinear harvesters, including multi-stable systems [21], [22]. A notable limitation, however, is the need for relatively large inductances to achieve proper matching, a constraint well-recognized in mechanical-to-electrical impedance matching [23]. Various circuit configurations can implement the matching network, many of which incorporate resonators to enable broadband impedance adaptation.

Broadband impedance matching is well-established in electronics and telecommunications, with a solid theoretical foundation, at least for AC systems. One effective method to achieve broadband matching is to couple multiple resonators in a ladder network [24]. Ladder networks have a mechanical analogue in chains of masses connected by elastic springs. This concept inspires the development of networked, multi-degree-of-freedom (multi-DOF) energy harvesters composed of coupled mass-spring elements, which can act as mechanical filters and be optimized to extract maximum energy from ambient vibrations. Adding mechanical DOFs improves power conversion efficiency while reducing the need for large inductors in the electrical matching circuits.

Motivated by this idea, this study investigates the design and optimization of a multi-DOF vibration energy harvester based on coupled resonators. In the proposed configuration, ambient mechanical vibrations are captured by a series of interconnected resonators that collectively function as a mechanical filter. Similar to an electrical filter, this system is designed to transmit specific frequency ranges while attenuating others, with the goal of maximizing harvested energy. Parasitic mechanical vibrations are modeled as a stochastic process. Linear system theory and the transmission matrix formalism are applied to derive analytical expressions for harvested power and conversion efficiency. Finally, a swarm intelligence algorithm is applied to optimize the mechanical resonator structure to maximize electrical power delivered to the load. Performance is demonstrated for devices with two and three mechanical DOFs, showing a notable increase in harvested energy.

The paper is organized as follows: Section II introduces the schematic representation of the networked energy harvester and derives the governing equations. In Section III we derive an equivalent circuit representation of the energy harvester. The analysis of the equivalent circuit in the frequency domain is discussed in Section IV. In Section V we introduce Particle Swarm Optimization and its application to the harvester. Section VI discusses the results. Finally, Section VII is devoted to the conclusions.

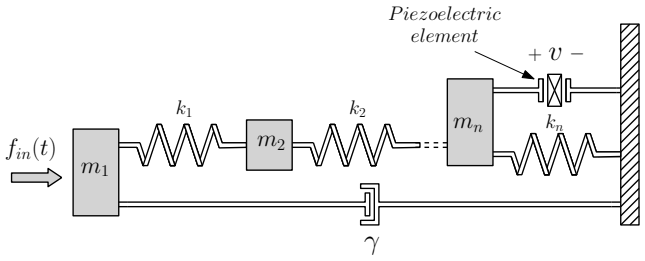

Fig. 1. Schematic representation of a networked multi-DOF resonator for energy harvesting applications.

II. Multi DOF energy harvester modeling

Figure 1 illustrates the schematic representation of the multi-DOF energy harvester proposed in this work. The device consists of a chain of mechanical resonators, where the masses $m_1, m_2, \ldots, m_n$ are connected pairwise by springs with stiffness constants $k_1, k_2, \ldots, k_n$. For simplicity, damping is assumed to act only on the first mass, modeled by a damper with coefficient γ. The piezoelectric element, attached to the terminal resonator, is responsible for transducing mechanical motion into electrical energy.

The coupling potentials due to the springs take the form:

$$U_j(x_j, x_{j+1}) = \frac{1}{2}\, k_j\, (x_j - x_{j+1})^2 \qquad j = 1, \ldots, n \quad (1)$$

where x_j is the displacement of the j-th mass from the rest position, and k_j is the elastic constant of the j-th spring. Each mass-spring couple represents one mechanical DOF, so that the chain has n-DOF. Since the last spring is connected directly to the transducer, we impose $x_{n+1} = 0$. The equation of motion for the j-th resonator is

$$m_j\ddot{x}_j + \gamma\dot{x}_j\delta_{1j} + k_{j-1}(x_{j-1} - x_j) + k_j(x_j - x_{j+1}) = f(t) \quad (2)$$

where δ_{ij} is Kronecker's delta function, and $f(t)$ is the force applied to the chains of mechanical resonators. This force is the resultant of the external force representing ambient mechanical vibrations, and of the force exerted on the resonator by the electrical load through the action of the transducer.

Ambient dispersed mechanical vibrations are typically random in nature, and therefore they are best described as stochastic processes. In real world applications most energy of mechanical vibration is concentrated at low frequencies, but for the sake of simplicity we shall assume that the frequency spectrum is wide enough, so that mechanical vibrations can be modelled as a white Gaussian noise [19]–[21].

For the transducer, we consider the constitutive equations for a linear piezoelectric material [25]:

$$\begin{bmatrix} \boldsymbol{S} \\ \boldsymbol{D} \end{bmatrix} = \begin{bmatrix} \boldsymbol{s^E} & \boldsymbol{d} \\ \boldsymbol{d}^T & \boldsymbol{\varepsilon^T} \end{bmatrix} \begin{bmatrix} \boldsymbol{T} \\ \boldsymbol{E} \end{bmatrix} \tag{3}$$

Here $\boldsymbol{S}$ and $\boldsymbol{T}$ are the mechanical strain and stress tensors, respectively. Symbols $\boldsymbol{D}$ and $\boldsymbol{E}$ are the dielectric displacement and electric field vectors, $\boldsymbol{s^E}$ and $\boldsymbol{d}$ are the compliance (evaluated at constant electric field) and the piezoelectric charge constants tensors. Finally, $\boldsymbol{\varepsilon^T}$ is the absolute permittivity evaluated at constant stress [26].

Through spatial integration of the microscopic description (3), a lumped parameter model describing the macroscopic behavior in terms of the mechanical force exerted by the transducer f_{tr}, displacement x of the mass connected to the transducer, charge q and voltage v, can be derived. In the quasi-static regime, neglecting the stiffness of the piezoelectric material, the governing equations are:

$$f_{\text{tr}}(t) = -\alpha\, v(t) \tag{4a}$$

$$q(t) = \alpha\, x(t) - C_{\text{pz}}\, v(t) \tag{4b}$$

where α is the electro-mechanical coupling (in N/V or As/m), and C_{pz} is the capacitance of the transducer. Taking the derivatives in (4b) and assuming that the load can be modeled as a resistor with conductance G_{L} we obtain:

$$\frac{\mathrm{d}v}{\mathrm{d}t} = \frac{\alpha}{C_{\text{pz}}}\frac{\mathrm{d}x}{\mathrm{d}t} - \frac{G_{\text{L}}}{C_{\text{pz}}}\, v \tag{5}$$

where $G_{\text{L}}\, v = dq(t)/dt$ is the current flowing through the electrical load.

III. Derivation of the equivalent circuit

Mechanical-to-electrical analogies permit to transform mechanical problems into electrical ones and vice versa, taking advantages of the methods and techniques developed in both domains. In the impedance analogy, masses are replaced by inductors, springs by capacitors, dampeners by resistors and forces by voltage sources. Using the substitutions summarized in table I, the governing equations can be rewritten in the form:

$$\frac{\mathrm{d}q_j}{\mathrm{d}t} = i_j \tag{6a}$$

$$\frac{\mathrm{d}i_j}{\mathrm{d}t} = -\frac{1}{L_j C_{j-1}}(q_j - q_{j-1}) - \frac{1}{L_j C_j}(q_j - q_{j+1}) + \frac{1}{L_j}\left(v_{\text{in}}(t) - R\, i_j\right)\delta_{j1} - \frac{1}{n_{\text{t}}\, L_j} v \delta_{jn} \tag{6b}$$

$$\frac{\mathrm{d}v}{\mathrm{d}t} = \frac{1}{n_{\text{t}}\, C_{\text{pz}}} i_n - \frac{G_{\text{L}}}{C_{\text{pz}}}\, v \tag{6c}$$

where $j = 1, \ldots, n$, and $n_{\text{t}} = \alpha^{-1}$ is the turns ratio of the ideal transformer.

Fig. 2 shows the equivalent circuit for the energy harvester with n mass-spring pairs. The external force modelling ambient mechanical vibrations is represented by the voltage source $v_{\text{in}}(t)$. For random vibrations, this voltage is modelled as a white Gaussian noise, and equations (6) becomes a system of stochastic differential equations[1]. The chain of mass-spring pairs is represented by the ladder of electrical resonators, composed by L-connected inductor and capacitor pairs. The piezoelectric transducer is represented by an ideal transformer, responsible for transferring energy from the mechanical domain to the electrical load, modeled by the resistor R_{L}. The capacitive behavior of piezoelectric material is described by the capacitor C_{pz}.

TABLE I
Mechanical-to-electrical analogy

Mechanical	Electrical
Displacement, x	Charge, q
Mass, m	Inductance L
Momentum $m\dot{x}$	Flux linkage, φ
Force, f	Voltage, v
Compliance, k^{-1}	Capacity, C
Damping, γ	Resistance, R

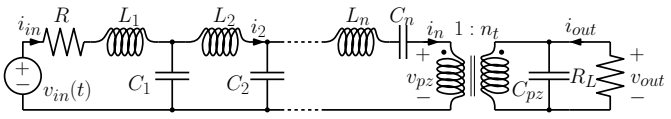

Fig. 2. Equivalent circuit for a multiple mass-spring pairs energy harvester for ambient mechanical vibrations.

IV. Equivalent circuit analysis

In the frequency domain, a linear time invariant (LTI) system is characterized by its input-output relationship:

$$S_Y(\omega) = |H(\omega)|^2\, S_X(\omega) \tag{7}$$

where $H(\omega) = \hat{Y}(\omega)/\hat{X}(\omega)$ is the transfer function, $\hat{Y}(\omega)$ and $\hat{X}(\omega)$ denote the Fourier transforms of the output and input signals, respectively, and $S_Y(\omega)$ and $S_X(\omega)$ are the corresponding power spectral densities (PSDs). The total output power is obtained by integrating the PSD over the entire frequency spectrum.

The input function represents the mechanical vibrations modeled as a white Gaussian noise with intensity D:

$$v_{\text{in}}(t) = D\, \frac{\mathrm{d}W_t}{\mathrm{d}t} \tag{8}$$

Consequently, the PSD for the input is:

$$S_{V_{\text{in}}}(\omega) = D^2 \tag{9}$$

Using (7) and (9), the average harvested power becomes:

$$P_{G_{\text{L}}} = G_{\text{L}}\mathrm{E}[v^2(t)] = \frac{D^2}{2\pi}\, G_{\text{L}} \int_{-\infty}^{+\infty} |H(\omega)|^2\, \mathrm{d}\omega \tag{10}$$

where $H(\omega) = \hat{V}_{\text{out}}(\omega)/\hat{V}_{\text{in}}(\omega)$ is the transfer function of the equivalent circuit.

[1]Since the noise is additive (or un-modulated), the stochastic equation can be interpreted indifferently as Itô or Stratonovich. We we will interpret all stochastic differential equations as Itô.

Similarly, the average power injected by the noise in the harvester is

$$P_{\text{in}} = \mathrm{E}[v_{\text{in}}(t)\, i_{\text{in}}(t)] = \frac{D^2}{2\pi} \int_{-\infty}^{+\infty} \mathrm{Re}[Y(\omega)]\, \mathrm{d}\omega \tag{11}$$

where $Y(\omega) = \hat{I}_{\text{in}}/\hat{V}_{\text{in}}$ is the input admittance, and $\mathrm{Re}[\cdot]$ denotes the real part.

The efficiency of the harvester is

$$\eta = \frac{P_{G_{\text{L}}}}{P_{\text{in}}} = G_{\text{L}} \frac{\int_{-\infty}^{+\infty} |H(\omega)|^2 \mathrm{d}\omega}{\int_{-\infty}^{+\infty} \mathrm{Re}[Y(\omega)] \mathrm{d}\omega} \tag{12}$$

To find the transfer functions, we use the transmission matrix formalism. The transmission, or $ABCD$ matrix $\mathbf{T}(\omega)$, defines the relationships between the input and output quantities:

$$\begin{aligned} \begin{bmatrix} \hat{V}_{\text{in}}(\omega) \\ \hat{I}_{\text{in}}(s) \end{bmatrix} &= \mathbf{T}(\omega) \begin{bmatrix} \hat{V}_{\text{out}}(\omega) \\ -\hat{I}_{\text{out}}(\omega) \end{bmatrix} \\ &= \begin{bmatrix} A(\omega) & B(\omega) \\ C(\omega) & D(\omega) \end{bmatrix} \begin{bmatrix} \hat{V}_{\text{out}}(\omega) \\ -\hat{I}_{\text{out}}(\omega) \end{bmatrix} \end{aligned} \tag{13}$$

For the resistive load of Fig. 2, $\hat{I}_{\text{out}} = -G_{\text{L}} \hat{V}_{\text{out}}$. Thus:

$$H(\omega) = \frac{\hat{V}_{\text{out}}}{\hat{V}_{\text{in}}} = (A(\omega) + B(\omega) G_{\text{L}})^{-1} \tag{14a}$$

$$Y(\omega) = \frac{\hat{I}_{\text{in}}}{\hat{V}_{\text{in}}} = \frac{C(\omega) + D(\omega) G_{\text{L}}}{A(\omega) + B(\omega) G_{\text{L}}} \tag{14b}$$

The equivalent circuit in Fig. 2 is composed by $n+1$ cascade connected two-ports, each one described by its own transmission matrix $\mathbf{T}_k(\omega)$. For cascade connected two-ports, the total transmission matrix is:

$$\mathbf{T}(\omega) = \prod_{k=1}^{n+1} \mathbf{T}_k(\omega) \tag{15}$$

The first stage of the transmission matrix describes the first mass-spring pair and the damper, corresponding to the first $R\, L_1\, C_1$ structure in Fig. 2. Using Kirchhoff current and voltage laws (KCL and KVL), the transmission matrix for the first stage is easily found as:

$$\mathbf{T}_1 = \begin{bmatrix} 1 + j\omega R C_1 + (j\omega)^2 L_1 C_1 & R + j\omega L_1 \\ j\omega C_1 & 1 \end{bmatrix} \tag{16}$$

where $j = \sqrt{-1}$.

Similarly, for the intermediate mass-spring pairs, represented by the $L_k\, C_k$ ladder stages, with $k = 2, \ldots, n-1$, the following transmission matrix is found:

$$\mathbf{T}_k = \begin{bmatrix} 1 + (j\omega)^2 L_k C_k & j\omega L_k \\ j\omega C_k & 1 \end{bmatrix} \tag{17}$$

The transmission matrix for the last mass-spring pair is:

$$\mathbf{T}_n = \begin{bmatrix} 1 & j\omega L_n + \dfrac{1}{j\omega C_n} \\ 0 & 1 \end{bmatrix} \tag{18}$$

Parameter	Value
R	0.12 Ω
D	10^{-3} V
$n_{\text{t}} = \alpha^{-1}$	238.0952
L_n	10 mH
C_n	1 mF
C_{pz}	80.08 nF
R_{L}	10 kΩ

TABLE II
VALUES OF THE EQUIVALENT CIRCUIT'S PARAMETERS FIXED IN THE ANALYSIS.

Finally, using KVL/KCL and the constitutive relationships of the ideal transformer the transmission matrix of the stage corresponding to the piezoelectric transducer is:

$$\mathbf{T}_{n+1} = \begin{bmatrix} 1/n_{\text{t}} & 0 \\ j\omega\, n_{\text{t}}\, C_{\text{pz}} & n_{\text{t}} \end{bmatrix} \tag{19}$$

Using (14)-(19), the transfer function for a energy harvester composed by an arbitrary number of mass-spring pairs can be calculated. The transfer function is then substituted into (10), (11) and (12) to find the average scavenged power and the power efficiency.

V. ENERGY HARVESTER OPTIMIZATION

We consider the problem of the optimization of the energy harvester. For the sake of simplicity and for a fair comparison with a single DOF energy harvester, we fix the value of some parameters, summarized in table II. The optimization is performed using the equivalent circuit and the results of section IV

The vector collecting the energy harvester's free parameters is denoted as $\boldsymbol{\mu} = [L_1, \ldots, L_{n-1}, C_1, \ldots, C_{n-1}]^T$. To make the comparison fair, we use fixed values for the last inductance L_n and the last capacitance C_n, equal to the values of L and C used for the single DOF harvester. The optimization problem is the following: Find

$$\boldsymbol{\mu}^* = \arg\max_{\boldsymbol{\mu} \in S} P_{G_{\text{L}}} \tag{20}$$

where $S \subset \mathbb{R}^{2n-2}$ is the parameter space.

Since the average harvested power and the power efficiency are found solving the integral equation (10), closed-form analytical expressions for the harvested power and its derivatives are not available. Therefore, gradient-based optimization methods are ill-suited for this problem.

Gradient free methods are widely used for solving complex optimization tasks efficiently, including Particle Swarm Optimization (PSO), inspired by the collective behavior of bird flocks or fish schools; Genetic Algorithms, inspired by natural selection; Simulated Annealing, based on the annealing process in metallurgy; and Ant Colony Optimization, which mimics how ants find shortest paths. Although many gradient-free methods could in principle solve the optimization problem, PSO is particularly well suited because of its effectiveness and reliability when the objective function must be evaluated numerically.

In particular, as a gradient-free algorithm, PSO does not require derivative information, it is simple to implement, requires minimal parameter tuning, and is inherently parallelizable, thereby enabling broad exploration of the search space while also effectively converging toward promising solutions through social learning mechanisms.

The original PSO algorithm was introduced in [27]. In its basic form, a swarm of N particles explores the parameter space seeking for the global minimum/maximum of the goal function [28]. Each particle position $\boldsymbol{\mu}_i$ and the corresponding velocity $\mathbf{v}_i$ are initialized at random, and for each iteration the best position that has been found for particle i is denoted as $\mathbf{p}_{i,\text{best}}$, while the best position that has been found for the whole swarm is denoted as $\mathbf{g}_{\text{best}}$. Each particle's velocity and position are updated as follows:

$$\begin{aligned}\mathbf{v}_i(t+1) = w\,\mathbf{v}_i(t) + c_1\,r_1\,(\mathbf{p}_{i,\text{best}}(t) - \boldsymbol{\mu}_i(t)) \\ + c_2\,r_2\,(\mathbf{g}_{\text{best}}(t) - \boldsymbol{\mu}_i(t))\end{aligned} \tag{21a}$$

$$\boldsymbol{\mu}_i(t+1) = \boldsymbol{\mu}_i(t) + \mathbf{v}_i(t+1) \tag{21b}$$

for all $i = 1\ldots, N$. Here, w is called the inertial weight, the hyper-parameters c_1 and c_2 are the cognitive and social acceleration coefficients, and r_1, $r_2 \in [0, 1]$ are two uniformly distributed random variables.

One of the computational advantages of PSO is that it can easily be parallelized. A large swarm of particles can be used to explore the parameter space, and the position and the velocity of each particle can be updated independently from, and in parallel with, all the others. The personal best and the global best are updated only once per iteration. PSO offers a good balance between exploration (the tendency to explore regions of the parameter space not visited before), and exploitation (the contrary tendency to focus on promising regions) [28].

VI. Results

We have applied PSO to the energy harvester with two, and three mechanical DOF described in Sec. II. The goal function to be maximized was the average harvested power P_{G_L} given by (10), where the transfer function is given in (14a), and the transmission matrix was found using (15)-(19).

As a reference, we show the results for the harvester with two mechanical DOF, because it allows for a clear visualization of trajectories in the parameter space P. Fig. 3 shows two examples of PSO trajectories. The average harvested power is shown, as a function of the inductance L_1, and of the capacity C_1. For the optimization the second inductance was fixed to $L_2 = 10.0$ H and the capacitance to $C_2 = 1$ F, to make a fair comparison with the single DOF system. The average output power has also been calculated using a grid search algorithm, shown in the figure as the background color. Only the trajectories of 20 particles chosen at random between the 50 composing the swarm are shown. The trajectories start from random initial positions, and converge rapidly to the same position in the parameter space, representing the maximum of the goal function.

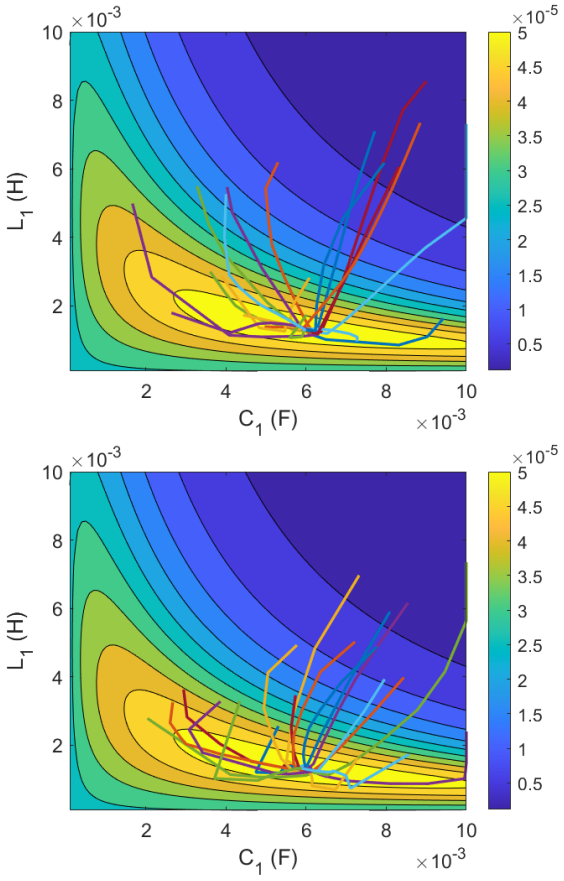

Fig. 3. Two examples of trajectories in the parameter space for PSO of an energy harvester with two mechanical DOF.

Table III summarizes the parameters of the multi DOF energy harvesters obtained through PSO, and the corresponding average harvested power. It turns out that increasing the number of mechanical DOF improves the power performance significantly, but offers diminishing returns. In particular, increasing the number of DOF from two to three offers very little increase in the harvested power, suggesting that increasing the number of DOF beyond three/four is not worth the additional complexity. The results prove that the three DOF energy harvester generates more than 100% additional power compared to the single mechanical DOF energy harvester.

Fig. 4 shows the amplitude responses for the harvesters with one, two and three mechanical DOF. It can be seen that the additional DOF produce a wider frequency bandwidth, at the cost of reduced amplitude at the resonant frequency. The efficiency of energy collection at the resonance frequency is reduced but, in exchange, more energy is collected at neighboring frequencies.

VII. Conclusions

We presented a methodology for the design and optimization of a multi-DOF energy harvester for ambient mechanical vibrations. The device consists of coupled mass-spring pairs, arranged to form a broadband mechanical resonator.

DoF	P_{out}	Parameters
1	28.74 μW	$L = 10$ mH $C = 1$ mF
2	53.70 μW	$L_1 = 1.30$ mH $L_2 = 10.0$ mH $C_1 = 6.0$ mF $C_2 = 1$ mF
3	58.15 μW	$L_1 = 0.70$ mH $L_2 = 2.60$ mH $L_3 = 10.0$ mH $C_1 = 10.0$ mF $C_2 = 3.10$ mF $C_3 = 1$ mF

TABLE III
AVERAGE HARVESTED POWER AND OPTIMUM VALUES OF THE FREE PARAMETERS.

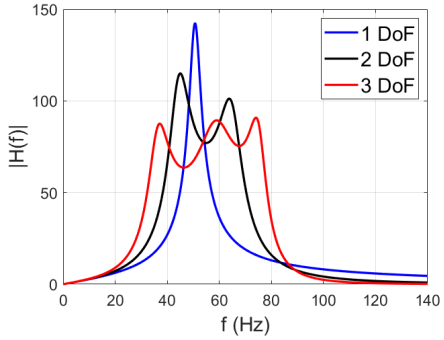

Fig. 4. Amplitude response for the networked energy harvester with one, two, and three mechanical DOF.

Starting from the governing equations, an equivalent electrical circuit was derived, enabling simplified analysis in the frequency domain. A transmission matrix representation was then introduced to compute the transfer function, the average harvested power, and the power conversion efficiency.

The optimization of the multi-DOF harvester was carried out using Particle Swarm Optimization. Since closed-form expressions for the average output power and its derivatives are not available, gradient-free methods such as PSO are particularly well suited for this problem. The algorithm proved both robust and efficient. Results show that the optimized multi-DOF harvester extracts significantly more powe – approximately a 100% increase, compared to a single-DOF system, thereby demonstrating the effectiveness of the proposed approach.

REFERENCES

[1] S. Roundy, P. K. Wright, and J. M. Rabaey, *Energy scavenging for wireless sensor networks*. Springer, 2003.

[2] J. A. Paradiso and T. Starner, "Energy scavenging for mobile and wireless electronics," *IEEE Pervasive Computing*, vol. 4, no. 1, pp. 18–27, 2005.

[3] R. Verdone, D. Dardari, G. Mazzini, and A. Conti, *Wireless Sensor and Actuator Networks*. Academic Press, 2008.

[4] M. F. Daqaq, R. S. Crespo, and S. Ha, "On the efficacy of charging a battery using a chaotic energy harvester," *Nonlinear Dynamics*, vol. 99, no. 2, pp. 1525–1537, 2020.

[5] S. Roundy and Y. Zhang, "Toward self-tuning adaptive vibration-based microgenerators," in *Smart Structures, Devices, and Systems II*, vol. 5649. SPIE, 2005, pp. 373–384.

[6] E. Blokhina, A. El Aroudi, E. Alarcon, and D. Galayko, "Nonlinearity in energy harvesting systems," *Micro-and Nanoscale Applications–Springer*, 2016.

[7] M. Rosso, A. Nastro, M. Baù, M. Ferrari, V. Ferrari, A. Corigliano, and R. Ardito, "Piezoelectric energy harvesting from low-frequency vibrations based on magnetic plucking and indirect impacts," *Sensors*, vol. 22, no. 15, p. 5911, 2022.

[8] F. Cottone, H. Vocca, and L. Gammaitoni, "Nonlinear energy harvesting," *Physical Review Letters*, vol. 102, no. 8, p. 080601, 2009.

[9] S. C. Stanton, C. C. McGehee, and B. P. Mann, "Reversible hysteresis for broadband magnetopiezoelastic energy harvesting," *Applied Physics Letters*, vol. 95, no. 17, 2009.

[10] A. Hajati and S.-G. Kim, "Ultra-wide bandwidth piezoelectric energy harvesting," *Applied Physics Letters*, vol. 99, no. 8, p. 083105, 2011.

[11] M. F. Daqaq, R. Masana, A. Erturk, and D. Dane Quinn, "On the role of nonlinearities in vibratory energy harvesting: a critical review and discussion," *Applied Mechanics Reviews*, vol. 66, no. 4, 2014.

[12] A. Arrieta, P. Hagedorn, A. Erturk, and D. J. Inman, "A piezoelectric bistable plate for nonlinear broadband energy harvesting," *Applied Physics Letters*, vol. 97, no. 10, p. 104102, 2010.

[13] F. Cottone, P. Basset, H. Vocca, L. Gammaitoni, and T. Bourouina, "Bistable electromagnetic generator based on buckled beams for vibration energy harvesting," *Journal of Intelligent Material Systems and Structures*, vol. 25, no. 12, pp. 1484–1495, 2014.

[14] S. Zhou, M. Lallart, and A. Erturk, "Multistable vibration energy harvesters: Principle, progress, and perspectives," *Journal of Sound and Vibration*, vol. 528, p. 116886, 2022.

[15] M. Bonnin, F. L. Traversa, and F. Bonani, "Colored noise in oscillators. phase-amplitude analysis and a method to avoid the ito-stratonovich dilemma," *IEEE Transactions on Circuits and Systems I: Regular Papers*, vol. 66, no. 10, pp. 3917–3927, 2019.

[16] ——, "Analysis of influence of nonlinearities and noise correlation time in a single-DOF energy-harvesting system via power balance description," *Nonlinear Dynamics*, vol. 100, no. 1, pp. 119–133, mar 2020.

[17] K. Song, M. Bonnin, F. L. Traversa, and F. Bonani, "A stochastic averaging mathematical framework for design and optimization of nonlinear energy harvesters with several electrical dofs," *Communications in Nonlinear Science and Numerical Simulation*, vol. 139, p. 108306, 2024.

[18] M. Bonnin, K. Song, F. L. Traversa, and F. Bonani, "Model order reduction and stochastic averaging for the analysis and design of micro-electro-mechanical systems," *Nonlinear Dynamics*, vol. 112, no. 5, pp. 3421–3439, 2024.

[19] M. Bonnin, F. L. Traversa, and F. Bonani, "Leveraging circuit theory and nonlinear dynamics for the efficiency improvement of energy harvesting," *Nonlinear Dynamics*, vol. 104, no. 1, pp. 367–382, 2021.

[20] M. Bonnin and K. Song, "Frequency domain analysis of a piezoelectric energy harvester with impedance matching network," *Energy Harvesting and Systems*, vol. 10, no. 1, pp. 119–133, mar 2022.

[21] M. Bonnin, F. L. Traversa, and F. Bonani, "An impedance matching solution to increase the harvested power and efficiency of nonlinear piezoelectric energy harvesters," *Energies*, vol. 15, no. 8, p. 2764, 2022.

[22] K. Song, M. Bonnin, F. L. Traversa, and F. Bonani, "Stochastic analysis of a bistable piezoelectric energy harvester with a matched electrical load," *Nonlinear Dynamics*, vol. 111, no. 18, pp. 16 991–17 005, 2023.

[23] B. Lossouarn, M. Aucejo, J.-F. Deü, and B. Multon, "Design of inductors with high inductance values for resonant piezoelectric damping," *Sensors and Actuators A: Physical*, vol. 259, pp. 68–76, 2017.

[24] M. M. Ahmad, N. M. Khan, and F. U. Khan, "Multi-degrees of freedom energy harvesting for broad-band vibration frequency range: A review," *Sensors and Actuators A: Physical*, vol. 344, p. 113690, Sep. 2022.

[25] "IEEE standard on piezoelectricity," 1988. [Online]. Available: https://ieeexplore.ieee.org/servlet/opac?punumber=2511

[26] S. Priya and D. J. Inman, *Energy harvesting technologies*. Springer, 2009, vol. 21.

[27] J. Kennedy and R. Eberhart, "Particle swarm optimization," in *Proceedings of ICNN'95-international conference on neural networks*, vol. 4. ieee, 1995, pp. 1942–1948.

[28] T. M. Shami, A. A. El-Saleh, M. Alswaitti, Q. Al-Tashi, M. A. Summakieh, and S. Mirjalili, "Particle swarm optimization: A comprehensive survey," *Ieee Access*, vol. 10, pp. 10 031–10 061, 2022.